MADRID
inter.noise 2019
June 16 - 19
NOISE CONTROL FOR A BETTER ENVIRONMENT

Design and Construction of a 2-D Phased Array Ultrasonic Transducer for Coupling in Water

Patricio Rodrigues, Estevão[1]
Francisco de Oliveira, Timoteo[2]
Yassunori Matuda, Marcelo[3]
Buiochi, Flávio[4]

Engineering School from University of São Paulo, Department of Mechatronic Engineering, Laboratory of Ultrasound, São Paulo, Brazil 05508-010.

ABSTRACT

Two-dimensional phased array transducers can deflect and focus the ultrasonic beam in a volumetric space, making a 3-D image reconstruction. In underwater media with low or no visibility, where underwater optical cameras become inefficient, this is an alternative approach to be used as tridimensional sonar. This paper presents the design, construction and characterization of a two-dimensional phased array ultrasonic transducer prototype for coupling in water. The transducer has sixteen elements arranged in a square matrix of 1-3 piezocomposite operating at 500 kHz. Improvements in sensitivity to echoes were reached with a quarter wavelength-thick matching layer and series inductors. Three types of backing layer material were simulated and tested for optimization of pulse-echo response: air, water and fiberglass. Images of objects at up to one-meter distance using the SAFT and TFM techniques were made, shown be feasible the use of the prototype constructed in underwater applications, like forward looking sonar and others in shallow waters.

Keywords: 3-D Sonar, Underwater, 2-D Phased Array.
I-INCE Classification of Subject Number: 00, 70, 76

1. INTRODUCTION

A 2-D phased array ultrasonic transducer can be used as a sonar to make feasible imaging in an opaque and low visibility medium, where optical cameras are not quite efficient. It is an array of elements made of a piezoelectric material that can be electronically controlled to transmit and receive acoustic beams. If the elements are excited with delays, a wavefront steered and focused at a given point is produced[1-4]. It is useful for underwater applications, such as for 3-D imaging cameras, and for forward looking sonar to find obstacle.

[1]estevaopatricio@usp.br [2]timoteolavras@gmail.com [3]marcelo@mym.eng.br [4]fbuiochi@usp.br

Some considerations should be taken for the transducer design. Unlike imaging applications as non-destructive inspections and clinical diagnostics, in underwater environment the objects of interest are very distant from the sonar (centimeters or meters), so the sonar operates at *far-field* given by[3,4] $r \geq L^2/4\lambda$, where r is a radial distance relative to the transducer face, L is the length of the transducer, and λ is the wavelength. In the far field, the elements act like a point source of spherical waves, and the electronic focalization with delay laws (phased array system) is inefficient for focusing and, therefore, the echoes arrive weak. Axial resolution is not a critical criterion because it is more important to detect the echoes from external surfaces of objects (like wrecked ship´s hull, sea floor, and bridge pillars) than internal structures.

Another important consideration for designing the transducer is the its operating frequency. The angular resolution, given by the Rayleigh criterion[5] as $\Delta\theta=\lambda/L$, determines the minimum angle required to resolve two objects spaced laterally at the same radial distance. It is improved with higher frequencies as long as the echoes are not highly attenuated.

The grating lobes are a spatial undersampling that occurs when the pitch is larger than [6-9] $\lambda/2$, producing false reflectors (artifacts) in the image[6,8,9]. A strategy to avoid them is to limit the steering of beam into an angular sector range, which can be calculated by[6,9] $\theta_{max}=\pm\arcsin(\lambda/2d)$.

A wide aperture array improves the angular resolution, but it is necessary to build a great number of elements or a large pitch (distance between the centers of two contiguous elements). Alternative approaches such as sparse arrays can reduce the number of elements required for a wide aperture and optimize the grating lobes, by breaking the periodicity of the elements. This is done by randomly removing $\lambda/2$ elements from a full matrix resulting in pitch larger than a half wavelength[10]. But, due to the lower number of elements, the noise level is higher[10,11,12]. In addition, when the element size is larger than $\lambda/2$ the non-periodic sparse array does not avoid the grating lobes, so the angular range of the image must be limited to avoid artifacts[6].

The sensitivity to detect echoes can be optimized with larger elements, using piezoceramics with low acoustic impedance and high electromechanical coupling. It is also important to use a backing layer with low acoustic impedance and low absorption, a matching layer for matching acoustic impedance, and series inductors for matching electrical impedance[2-4]. Not only the sensitivity, but also the bandwidth should be as high as possible for increasing the range of echoes detection and for reducing the grating lobes[7]. A wide bandwidth allows the implementation of the SCF (*Sign Coherence Factor*) technique[8] to reconstruct images with few or no artifacts and to reduce the noise level.

2. DESIGN OF THE 2-D PHASED ARRAY TRANSDUCER

In this paper, the 2-D phased array for coupling in water is constituted mainly by a 4x4 matrix of elements of 1-3 piezocomposite, a matching layer, a backing layer, a foam housing and wires for electrical interconnections (Figure 1).

The piezoelectric ceramics converts electrical energy into acoustical energy and vice versa (piezoelectric effect)[1-4]. The matching layer is used to match the acoustic impedance of the 1-3 piezocomposite matrix to the acoustic impedance of the water. This improves the bandwidth, and the emission and the reception of signals[2-4]. The backing layer can be designed to absorb the waves that propagated backwards, such that the bandwidth is improved. It can also be designed to reflect those waves forward to increase the energy

transmitted at the cost of reducing the bandwidth[3]. The transducer parts are mounted inside a foam housing, keeping it isolated from environment acoustic disturbances.

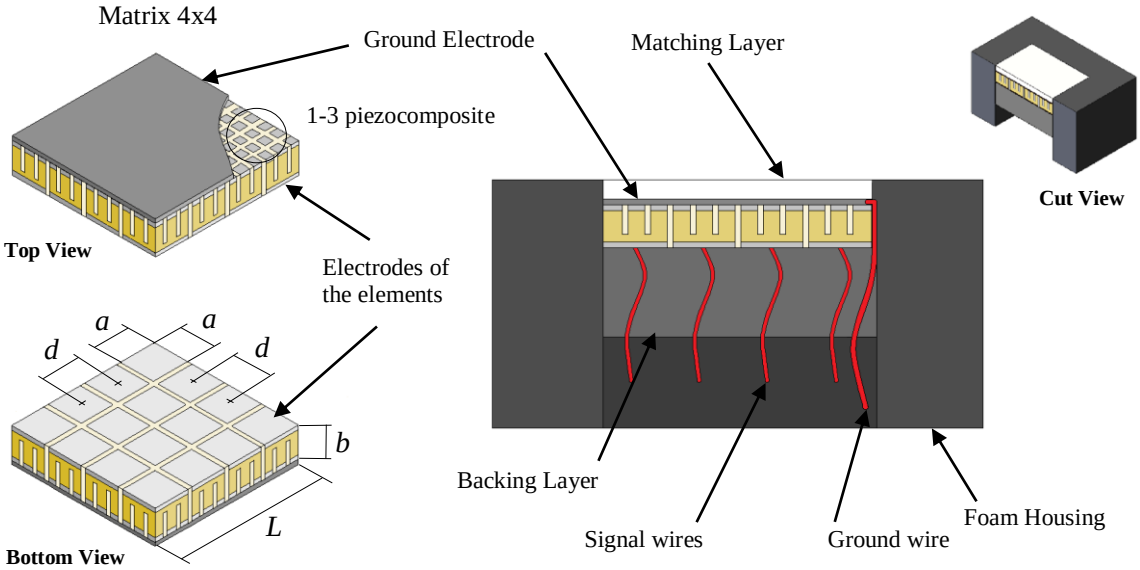

*Figure 1 - Main parts of the 2-D phased array ultrasonic transducer for coupling in water. The matrix dimensions are a=5mm, d=*5.2mm*, b=2.8mm, and L=20.6mm. To better visualization some dimensions are out of scale.*

2.1 Design of the array of 1-3 piezocomposite

The square geometry simplified the fabrication of the matrix of elements as used in 3D sonars[13,14]. In this work, the matrix has sixteen elements arranged in a 4x4 matrix. This amount of elements is much smaller than that found in most 3-D underwater sonars, which have hundreds or even thousands of elements[6,13,14]. However, it was enough to deflect and to focus the acoustic beam, making 3-D images, at the cost of low resolution $\Delta\theta \approx 8^o$. Furthermore, the SCF method can be improved the angular resolution by two times[8], therefore, the lateral resolution is improved to 4^o with this technique.

The elements size is limited by the pitch, which is d=5.2mm≈1.7λ. This pitch size is within the works found in the literature of 2-D array transducers[6,7,9], generally $\lambda \leq d \leq 2\lambda$. The dimensions of the square elements are a=5mm (equal sides) and b=2.8mm (thickness). The gap between the elements is determined by the thickness of the saw blade t_{saw}=200µm, resulting in a 4x4 matrix with side equal to L=20.6mm (Figure 1).

The deflection and focus were simulated with the geometries chosen for the transducer with a software developed in Matlab®. The software is based on an analytical solution of the Rayleigh integral, which evaluates the impulse velocity potential of rectangular transducers modeled as rigid pistons[15]. Two types of transient excitation were used to simulate the acoustic field: narrowband (20% of bandwidth), and wideband (50% of bandwidth). The function of the excitation pulse is given by[15] $vn(t)=Ct^3e^{-kft}\cos(2\pi ft)$, where C is a constant amplitude, t is the time, f is the frequency, and k=1.437 for 20% of bandwidth, and k=3.833 for 50% of bandwidth. The simulations indicate that grating lobes increase, and they are away from the main lobe to the narrowband excitation pulse (Figure 2a). The wideband excitation pulse seems more suitable for the array geometry designed, showing lower grating lobes level (Figure 2b). The beam was deflected to 15^o relative to the acoustic axis (z axis), close to the maximum theoretical to avoid grating lobes which is $\theta_{max}=16.5^o$.

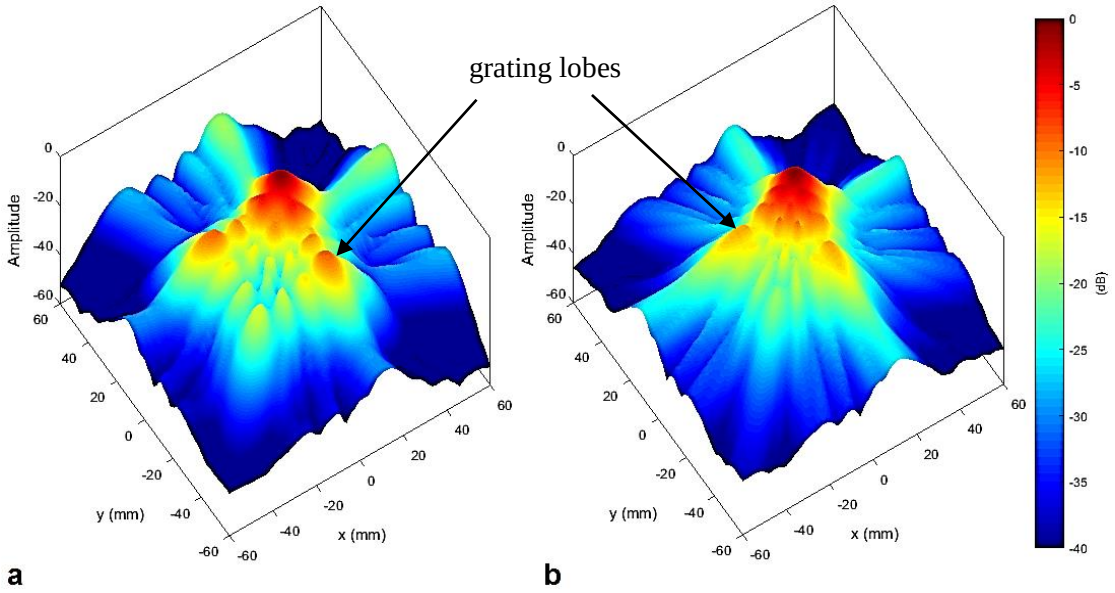

Figure 2 - The acoustic field of the 2-D phased array was simulated at a parallel plane at 50mm (far field) from the transducer face. The beam was deflected at θ=15º and φ=45º *with narrowband (a) and wideband (b) excitations, respectively.*

The aspect ratio criterion to make the array elements operate preferably in thickness vibration mode rather than lateral coupled modes is given by $a/b \leq 0.6$ (pillar or rod aspect) or $a/b \geq 10$ (disc or plate aspect), where a and b are the lateral dimension and the thickness of the element, respectively[2]. For a pure Pz37 ceramic, the designed geometries gives a/b=5mm/2.8mm=1.8. To satisfy this criterion the 1-3 piezocomposite was chosen as an alternative[16,17] (Figure 3). Each element was divided in nine pillars of sides $a_{1\text{-}3}$=1.53 mm and pitch $d_{1\text{-}3}$=1.73mm, resulting in an aspect ratio of $a_{1\text{-}3}/b$=0.55.

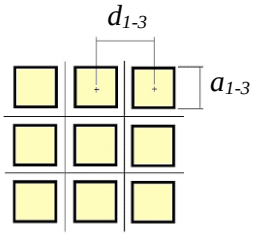

Figure 3 - The elements of 1-3 piezocomposite are constituted of a group of nine Pz37 pillars filled with epoxy resin. The dimensions $a_{1\text{-}3}$=1.53mm and $d_{1\text{-}3}$=1.73.

The matrix made with the 1-3 piezocomposite also allowed to optimize the acoustic coupling with water due to the low acoustic impedance, besides offering a better electromechanical coupling in the thickness mode k_t, and low electrical and mechanical losses than a pure PZT piezoelectric ceramics or piezoelectric polymers[16].

The 1-3 piezocomposite has two phases, one of piezoceramic (active) and another from polymer (passive). A Pz37 piezoceramic from Ferroperm™ Meggitt A/S, with frequency of 500kHz, was utilized to make the active phase, and the Araldite® GY 279 and hardener Aradur® 951 was utilized to make the passive phase. The Pz37 ceramic has low acoustic impedance of 18Mrayl, being adequate for underwater applications[18].

To models the 1-3 piezocomposite as a homogeneous material the lateral periodicity of the pillars must be fine enough, much smaller than all relevant acoustic wavelengths[16]. The relative quantity of ceramic into 1-3 piezocomposite was computed in fraction of volume as[17] $\delta_{Pz37}=a_{1\text{-}3}^2/d_{1\text{-}3}^2$, resulting in 78% of Pz37. The 1-3 piezocomposite properties

were simulated in Matlab® (Figure 4), using an approached model[16]. According to the simulations, considering δ_{Pz37}=0.78, it is expected that the acoustic impedance of the elements decreases by 16%, from 18Mrayl to 15.2Mrayl, and the k_t increases by 6%, from 0.54 to 0.57. These results improve the echoes responses, due to the optimization of acoustic and of electromechanical coupling, respectively.

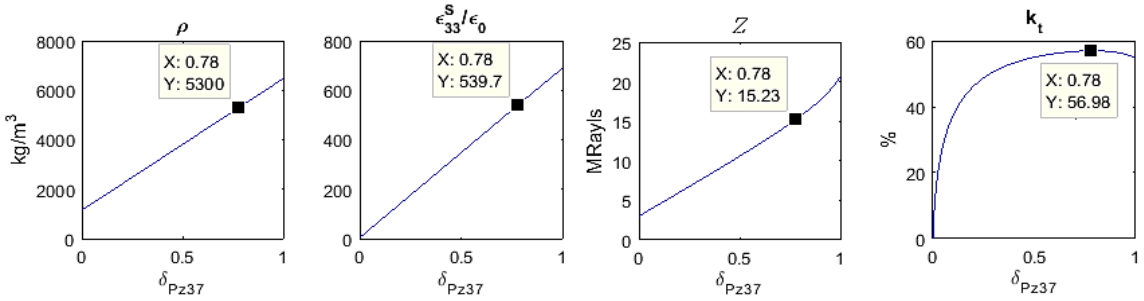

Figure 4 - The 1-3 piezocomposite properties were simulated, and the values at 78% were taken to design the matching layer and to electroacoustic simulations using the KLM model.

2.2 Design of the matching layer

The acoustic impedance of the matching layer Z_m was calculated by the geometric mean of the acoustic impedances[1-4,7] of water and 1-3 piezocomposite. The quantity of alumina powder necessary to make the composite, given in volume fraction, and the acoustic wave velocity to calculate the matching layer thickness, given by a quarter of the wavelength, was taken directly from the graphics (Figure 5), that was simulated by an approached model[19]. Initially, was localized the volumetric fraction of alumina powder δ_{Al}=30% corresponding to Z_m=4.8Mrayl (Figure 5a). Next, the longitudinal wave speed is determined directly from the alumina volume fraction (Figure 5b). Then, the matching layer thickness is computed as $b_m=c_m/f/4$=1.48mm.

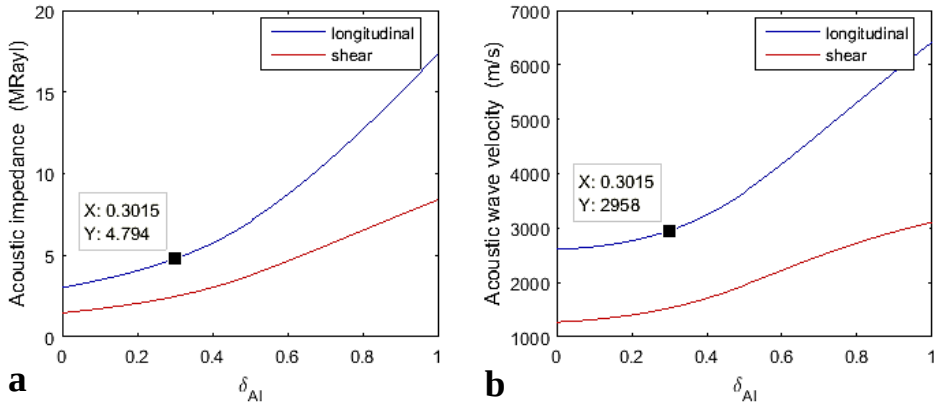

Figure 5 - The amount of alumina powder to make the matching (a), and the velocity of the acoustic wave to calculate its thickness (b) were obtained from the simulated curves.

2.3 Design of the backing layer

When an acoustic wave traveling in one medium (with a given acoustic impedance, $Z=\rho c$, where Z is the acoustic impedance, ρ is the density, and c is the wave speed) intercepts an interface of a second medium (with different acoustic impedance), a partial reflection and transmission of the wave occur. On the other hand, if both acoustic impedances are equal, the transmission is total and no reflections occur[1-4,7]. The knowledge of this physical phenomena is useful for design the backing layer.

According to the intensity transmission and reflection coefficients present in Table 1, $T_i=4Z_1Z_2/(Z_1+Z_2)^2$ and $R_i=1-T_i$ are calculated[1-4,7,19], respectively (where Z_1 and Z_2 are the acoustic impedances of the 1-3 piezocomposite and of the backing layer, respectively). If an air backing layer is utilized, all waves that propagated backwards will be reflected to forward, optimizing the emission. If a fiberglass backing layer is used, the emission is lower than that from the air backing, but the bandwidth is expected to improve. At the end, if no backing layer is used and the back face of transducer is coupled directly to the water, an intermediate emission performance is obtained. Generally, the lower is the backing layer acoustic impedance, the higher is the emission, and the lower is the bandwidth[3].

Table 1 – Material properties to design the backing layer

Material		c (m/s)	ρ (kg/m^3)	Z (Mrayl)	*Ti*	*Ri*
Z_1	Composite1-3, δ_{PZ37}=0.78	2874	5300	15.23	-	-
Z_2	Air	330	1.2	0.0004	0	1
	Water	1480	1000	1.48	0.32	0.68
	Fiberglass*	2344	1086	2.55	0.49	0.51

*Sample made with fiberglass of 0.13g/cm^3 and Araldite® AW106 with hardener HV953U

2.4 Design of the electromechanical responses model

The 2-D array transducer was modeled as a matrix composed of individual elements, therefore, the physical interconnections between the elements that make cross-talk effects were disregarded. The one-dimensional model implemented in Matlab® describes the piezoelectric transducer like a transmission line, which has one electrical and two mechanical (acoustic) ports, known KLM model[20] (Figure 6). Each one of the transducer parts has a *T* matrix transfer, also known as ABCD matrix[4,20-22]. Dielectric and mechanical losses were inserted with *tan(δ)* and mechanic quality factor *Q*[22].

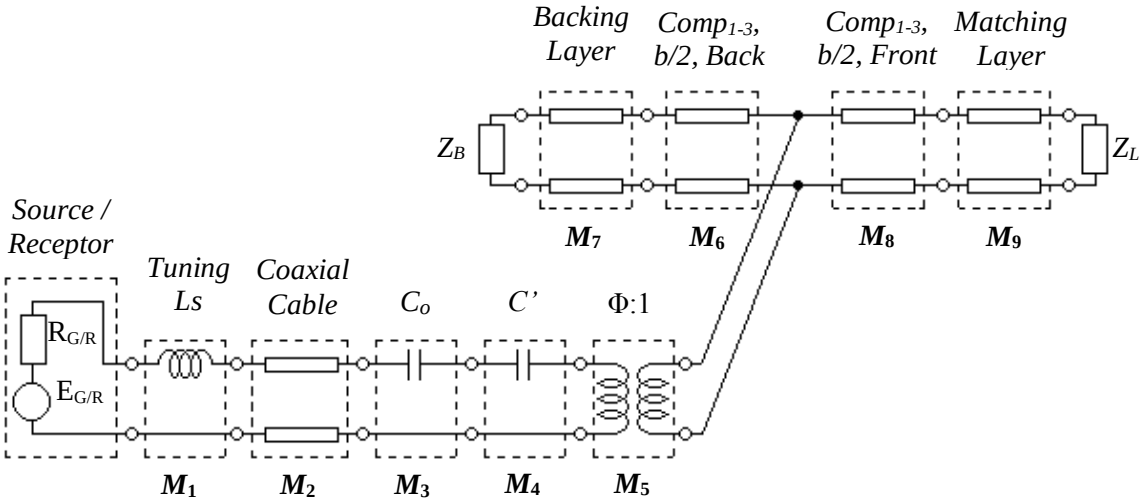

Figure 6 - Schematic of the piezoelectric transducer modeled as transmission line

The total transfer function is given by the matrix M_T, computed by multiplications of square matrix as $M_T=M_{electric}M_{mechanic}$, where $M_{electric}=M_1M_2M_3M_4M_5$ and $M_{mechanic}=[M_7M_6]_{par}M_8M_9$. The "*par*" index means that the multiplication result must be convert in a parallel impedance to the center tap before continuing the multiplications[22]. The Z_B and Z_L are the backing and the load acoustic impedances, given by Z_BA and Z_LA, respectively, where A is the area of the element. Because the transducer operates in water, Z_B and Z_L are 1.5Mrayl.

3. CONSTRUCTION OF THE 2-D PHASED ARRAY TRANSDUCER

The construction began with the fabrication of the 4x4 matrix of piezoceramic. The plate of Pz37 ceramic was diced in orthogonal directions, with a semiautomatic cutting precision machine ISOMET 4000 (Figure 7a), separating the elements with steps of 5.2mm and the inter-element spaces were filled with epoxy resin (Figure 7b). Using the dice-and-fill technique the 1-3 piezocomposite elements were made with pitch of 1.73mm, leaving a thin ceramic layer of 200μm to keep the electrodes of the elements. The cutting process resulted in nine pillars for each element of the array (Figure 7c). The electrodes of each nine pillars belonging to an array element were joined with conductive resin CW2400 Chemtronics®.

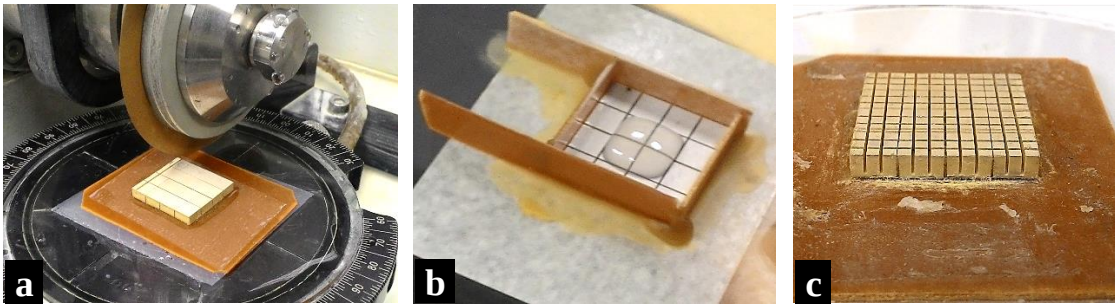

Figure 7 – The 2-D 4x4 array was made dicing the Pz37 plate in orthogonal directions (a) and filling the kerfs with epoxy resin (b). Finally, the 1-3 piezocomposite was made by repeating the dice-and-fill process with smaller steps and leaving a thin layer to keep the electrodes (c).

The matching layer was formed by mixture of alumina powder embedded in an epoxy resin. The composite was deposited over the ground electrode of the transducer array (Figure 8a). After the cured resin, the composite was manually sanded on the rotary sanding machine until the matching layer thickness equal to 1.48mm was obtained (Figure 8b, c).

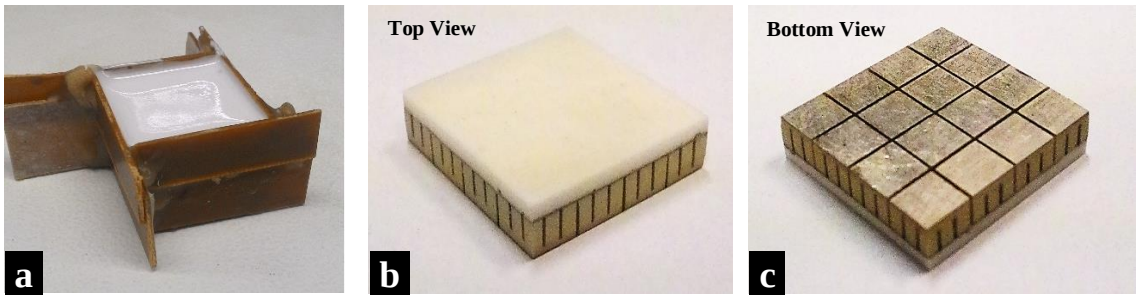

Figure 8 – The alumina composite was deposited over the ground electrode (a), and after it cured, the composite was sanded until the λ/4 thickness. At this stage, the transducer was ready to solder the wires, and to be encapsulated with a foam housing (b), (c).

All the electrical interconnections of elements were made with enameled wires of diameter equal to 150μm. One end of the wire was soldered onto the electrode of the element, and the other end was soldered onto the signal connector of the board (Figure 9a). The housing was made of EVA foam tape, which were cut into four strips and bonded with Super Bonder Instant Adhesive *LOCTITE*®. The backing layer of air was obtained closing the back of the transducer with a transparent acrylic plate bonded with silicon hot glue. A board with axial 330μH series inductor is fit into the multicoaxial cable to matching the electrical impedances. The accomplished 2-D phased array prototype transducer is shown in Figure 9b.

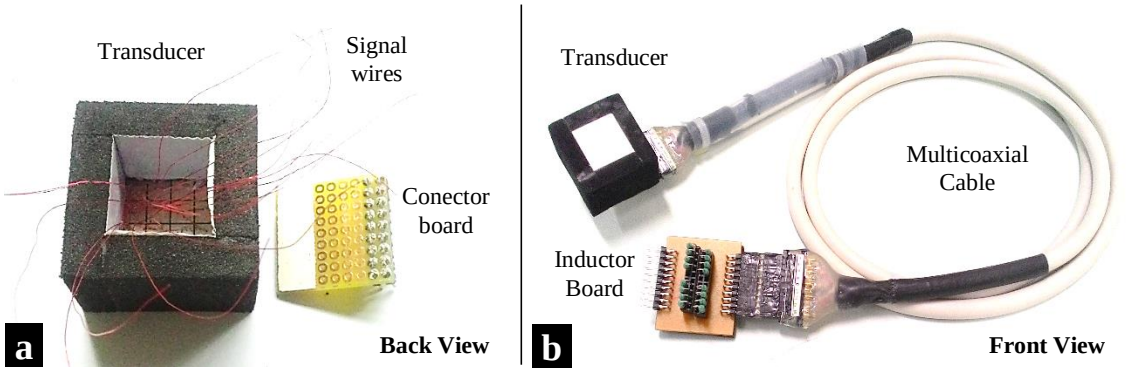

Figure 9 - Enameled 150μm wires was soldered on electrodes(a); transducer accomplished(b).

4. CHARACTERIZATION AND OPTIMIZATION

4.1 Electrical impedances

The electrical impedances of each element of the air backing transducer, with the multicoaxial cable, were measured in water with an Agilent 4294A impedance analyzer. The average of the electrical impedance at resonance series frequency measured was $|Ze|=1274\Omega^{\pm 290}|\underline{-82}^{o\pm 14}$ @ 520kHz$^{\pm 98}$ and the simulated was $|Ze|=1300\Omega|\underline{-80}^{o}$ @ 514kHz.

The matching series inductors, *Ls*, improve the transfer of energy between the transmitter, which has low impedance (50 Ω), and the elements of the transducer, which have very higher impedance[2,4].

At resonance frequency, f_o, to null all the reactive capacitances, X_C, of the transducer including cable, connectors, soldering and others, the series inductor was calculated as $X_C=X_L=\text{imag}(Ze)$, then $C=1/(\omega_o X_C)=1/(\omega_o \text{imag}(Ze))$ and[2-4] $L=1/(\omega_o^2 C)$. Hence, the experimental and simulated capacitances and series inductors are C_{exp}=242.6pF and Ls_{exp}=386μH, and C_{sim}=241.9pF and Ls_{sim}=396μH, respectively.

Excellent results were obtained with commercial axial inductors of 330μH, as example, the matched magnitude impedance at resonance frequency (where the phase was nulled) of the element 10 decreased to 134Ω @ 592kHz and the simulated decreased to 137Ω @ 580kHz (Figure 10).

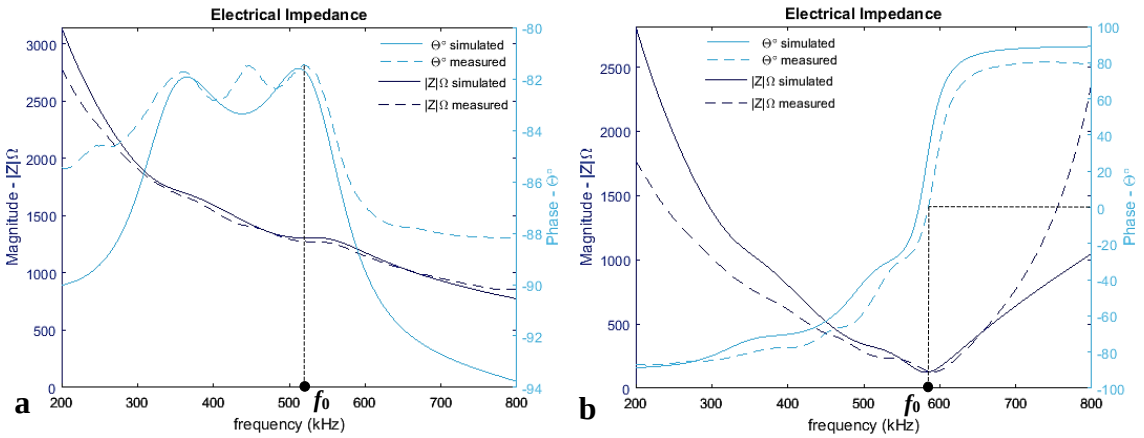

Figure 10 – Electrical impedances measured of the element 10 (dashed lines) and simulated (continuous lines) with no matching series inductor (a) and with 330μH series inductor (b).

4.2 Electroacoustic responses

The pulse-echo measurements were made with an Olympus Panametrics NDT 5077PR square wave pulser/receiver, that was configured for all measurements to 100 Hz of pulse repetition frequency, 100V negative square pulse, 500kHz transducer frequency, 0dB

gain, high pass frequency disabled, and 10 MHz low pass filter. The echoes of a reflector of brass at 50mm from the transducer face were acquired with an Agilent Infiniium MSO8104A 1GHz. The sampling frequency of 50MHz was utilized both in the electromechanical and acoustic field simulations as in the measurements.

The software to simulations of the electroacoustic responses was validated with comparisons with measurements made with a central element of the array (Figure 11) and the main results are presents in the Table 2.

Table 2 – Time and frequency responses with three backing layer types

Type of Backing Layer			Air		Water		Fiberglass
Measurement			Measured	Simulated	Measured	Simulated	Simulated
Peak-to-Peak Voltage		mV	210 ± 33	202	138 ± 18	154	133
Bandwidth		%	53 ± 1	52	57 ± 9.4	53	44
Central Frequency - f_o		kHz	479 ± 4.8	496	468 ± 4.6	493	507
Angular resolution (est.)	Rayleigh	º	8.7	8.4	8.9	8.5	8.2
	SCF	º	4.4	4.2	4.5	4.3	4.1
Angular view @-3dB (est.)		+/- º	17.5	16.9	17.9	17	16.5

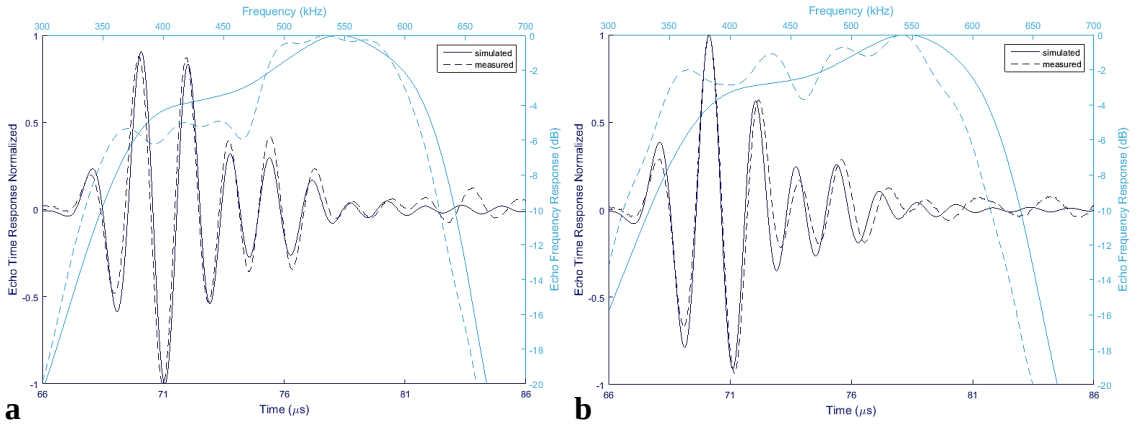

Figure 11 – The echoes responses in the time and frequency domain were simulated (continuous line) and compared with the measured (dashed line) of element 10, with air backing (a) and water backing (b), both matched with 330μH series inductors and normalized voltages.

5. IMAGES FROM REFLECTORS IMERSED IN WATER

Two flat reflectors, positioned parallel to the transducer face, spaced apart longitudinally and laterally, were imaged with the transducer with air backing layer, with the SAFT (Synthetic Aperture Focusing Technique) and TFM (Total Focusing Method) post-processing, implemented in Matlab®. In both techniques the beam was dynamically focused at all points of the volume of interesting (VOI), and the *Sign Coherence Factor*[8] was implemented to minimizes the grating lobes, the noise and to improve the lateral resolution.

Each object is shown as a cloud of points. The color bar indicates the radial distance between the center of the transducer to the reflectors, where nearby objects are plotted in red color, and distant objects are plotted in blue color. The real objects were plotted with the correspondent images colors.

The VOI was restrained by the length and the width of the tank, of 1.4m and 0.6m, respectively, and the water depth of 0.2m (Figure 12). The sampling window was limited between r_i=0.95m and r_f =1.25m, to optimize the amount of data to processing (Figure 13). The azimuth and elevation angles were θ=±15º *and* φ=±4º, and the discretizions

were $\Delta\theta$=0.5º, $\Delta\varphi$=0.5º, and $\Delta r=\lambda/12$. The real scenery and its virtual model are depicted in Figure 12 and Figure 13, respectively.

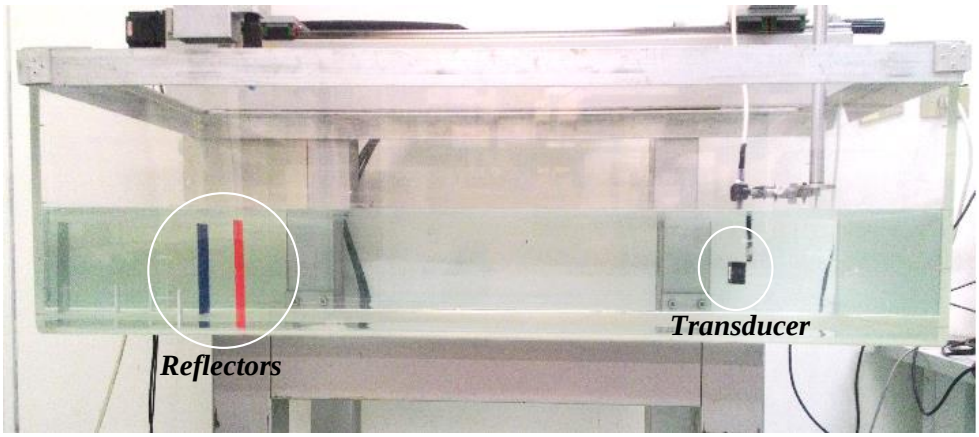

Figure 12 - Two rectangular reflectors (60x160mm) immersed in a tank, positioned parallels to the transducer face, at radial distances of 1m (red) and 1.15m (blue), interspaced of $\theta_{objects}$=8.6º

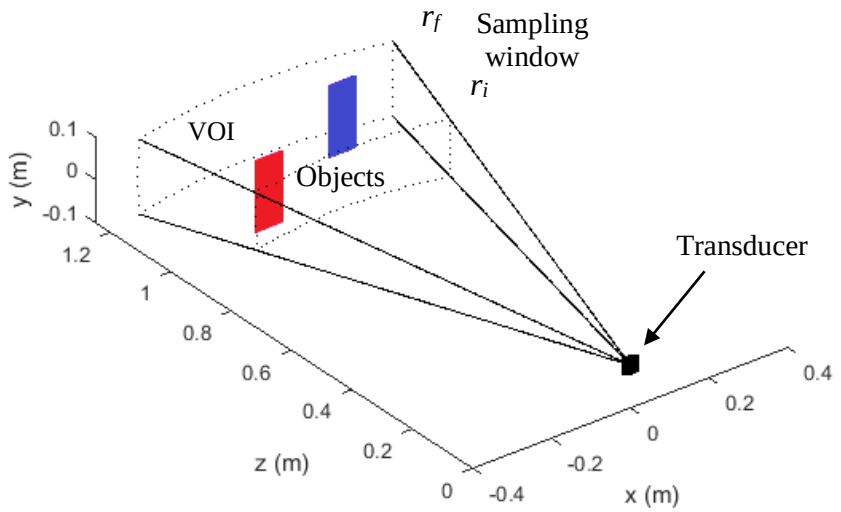

Figure 13 – The virtual scenery reproduces the objects (red and blue) inside of the VOI (volume of interesting), which was restrained in θ=±15º, φ=±4º and r=[0.95:1.25]m (sampling window).

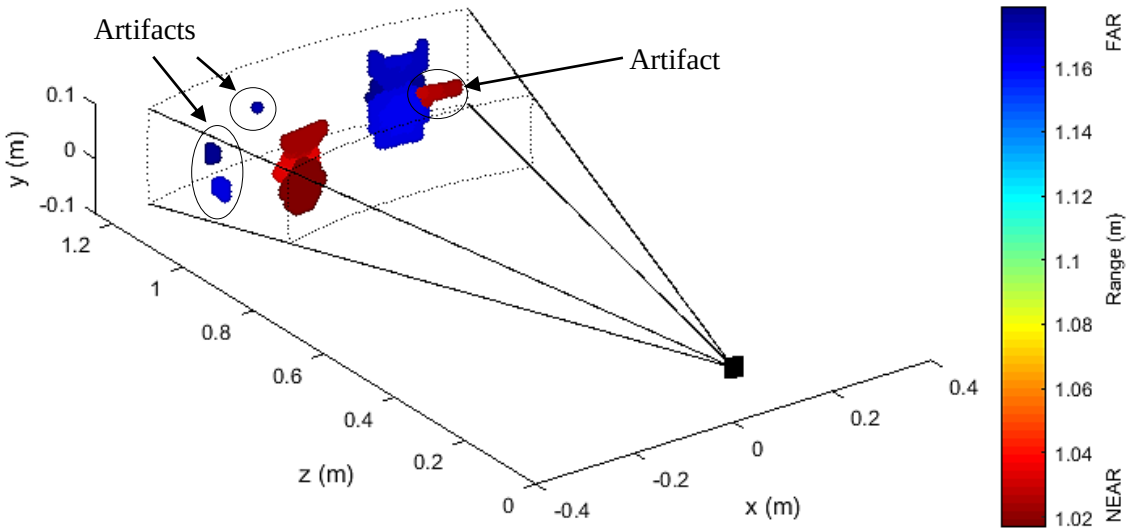

Figure 14 – The SAFT image with threshold equal to -7dB and 0.2 SCF coefficient, still present artifacts due the grating lobes.

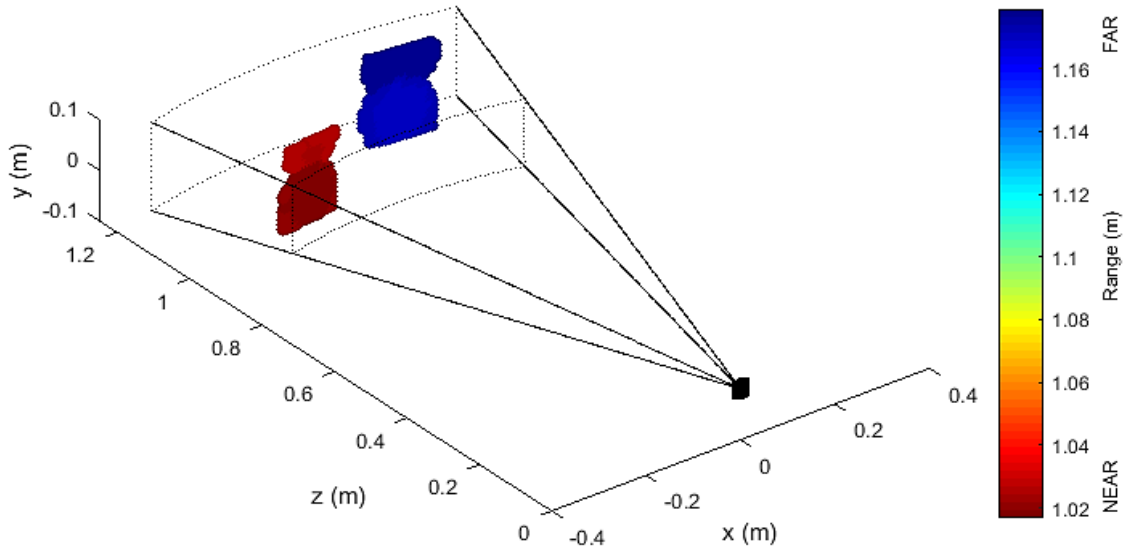

Figure 15 – The TFM image with threshold equal to -40dB and 4.5 SCF coefficient, no presents artifacts and the object geometry is better identified.

6. CONCLUSIONS

A 2-D phased array ultrasonic transducer for coupling in water was designed, constructed and characterized. The electrical matching with series inductors lowered up to ten times the electrical impedance, improving the energy transmission between the transducer and the transmitter/receptor, optimizing the echoes responses.

The transducer with backing layer of air provides the highest sensitivity over all others, with little loss in the bandwidth. The transducer with water backing layer and the one simulated with fiberglass backing were 24% and 34%, respectively, less sensitivity than with air backing, with almost no improvement in the bandwidth. Thus, an air backing layer seems more adequate for underwater applications to detect distant reflectors.

The process of images obtained by SAFT is faster than that obtained by TFM, at the cost of high noise level and narrow dynamic range (minimal threshold equal to or higher than -7dB) to avoid artifacts that arise from grating lobes. The TFM technique requires the storage of 256 signals while the SAFT technique stores only 16 signals. Although, the TFM is 30 times slower to process, the image quality is better, allowing deeper dynamic range. The artifacts were totally removed in the TFM image, because the SCF algorithm calculates the mean of the signals polarities at a given image point.

The results are promising for submarine applications, such as 3-D forward looking sonar, because the prototype constructed allowed to detect and image objects up to 1.15m apart from the sonar. In the near future, more experiments will carried out with fiberglass backing layer in order to operate the transducer in deep waters. A new 2-D phased array prototype with more elements will be developed to study other approaches of 3-D underwater imaging.

7. ACKNOWLEDGEMENTS

The authors acknowledge to CAPES, CNPq, FAPESP (grant #2017/13094-4) and Petrobras for their financial support to this research.

8. REFERENCES

1. Butler, J. L. and Sherman, C. H., *"Transducers and arrays for underwater sound"*, Springer International Publishing (2016).
2. Bronzino, J. D., "*Biomedical engineering handbook"*, CRC press, United States, third edition (2006).
3. Cheeke, J. D. N., "*Fundamentals and Applications of Ultrasonic Waves"*, Second Edition, pp122 (2012).
4. Szabo, T. L.,*"Diagnostic ultrasound imaging: inside out"*, Academic Press, (2004).
5. Suarez, J. R., Marich, K. W., Holzemer, J. F., Taenzer, J., "*Acoustical Holography: Volume 6*", Springer, Boston, MA (1975).
6. Trucco, A., Palmese, M., and Repetto, S., *"Devising an affordable sonar system for underwater 3-D vision"*, IEEE Trans. Instrum. Meas., vol. 57, no. 10, pp. 2348–2354 (2008).
7. Ensminger, D. and Stulen, F. B., *"Ultrasonics: data, equations and their practical uses"*, CRC press, (2008).
8. Camacho, J., Parrilla, M., Fritsch, C., *"Phase coherence imaging"*, IEEE transactions on ultrasonics, ferroelectrics, and frequency control, v. 56, n. 5, (2009).
9. Istepanian, R. S. H., and Stojanovic, M., *"Underwater acoustic digital signal processing and communication systems"*, Boston, MA: Kluwer Academic Publishers (2002).
10. Turnbull, D. H., & Foster, F. S., *"Beam Steering With Pulsed 2-Dimensional Transducer Arrays"*. IEEE Transactions on Ultrasonics Ferroelectrics and Frequency Control, 38(4), 320–333. https://doi.org/10.1109/58.84270, (1991).
11. Lockwood, G. R., Li, P. C., O'Donnell, M., & Stuart Foster, F., *"Optimizing the radiation pattern of sparse periodic linear arrays". IEEE Transactions on Ultrasonics, Ferroelectrics, and Frequency Control*, *43*(1), 7–14. https://doi.org/10.1109/58.484457 (1996).
12. Shung, K. K., *"DIAGNOSTIC DIAGNOSTIC Flow Measurements"*, (2006).
13. Ehrhardt, M., Becker, F. J., Speicher, D., Fonfara, H., Hewener, H., Fournelle, M., Tretbar, S., *"Evaluation of a high-resolution real-time capable 3D sonar camera for deep sea operation"*, OCEANS 2016 MTS/IEEE Monterey, OCE 2016, 19, 101–110. https://doi.org/10.1109/OCEANS.2016.7761232, (2016).
14. http://www.farsounder.com/products/navigation_sonars, accessed in (02/2019).
15. San Emeterio, J. L. and Ullate, L. G., *"Diffraction impulse response of rectangular transducers"*, The Journal of the Acoustical Society of America, 92(2), 651-662, (1992).
16. Smith, W. A. and Auld, B. A., *"Modeling 1-3 composite piezoelectrics: thickness-mode oscillations"*, IEEE transactions on ultrasonics, ferroelectrics, and frequency control, v. 38, n. 1, p. 40-47, (1991).
17. Hayward, G., & Bennett, J., *"Assessing the influence of pillar aspect ratio on the behavior of 1-3 connectivity composite transducers"*, IEEE Transactions on Ultrasonics, Ferroelectrics, and Frequency Control, 43(1), 98-108, (1996).
18. https://www.meggittferroperm.com/, accessed in (02/2019).
19. Sayers, C. M. and Tait, C. E., "*Ultrasonic properties of transducer backings*", Ultrasonics, 22(2), 57–60. https://doi.org/10.1016/0041-624X(84)90022-2, (1984).
20. Krimholtz, R., Leedom, D. A., & Matthaei, G. L., "*New Equivalent Circuits for Elementary Piezoelectric Transducers*", *Electronic Letters*, *6*(13), 398–399. https://doi.org/10.1049/el:19700280, (1970).
21. San Emeterio, J.L., Sanz, P.T., Riera, E. and Ramos, A., *"Una implementación del modelo KLM para transductores piezoelectricos en modo espesor"*, Anales Fisica B, 84, pp. 48–55, (1988).
22. Oakley, C. G., *"Calculation of ultrasonic transducer signal-to-noise ratios using the KLM model"*, IEEE Transactions on Ultrasonics, Ferroelectrics, and Frequency Control, 44(5), 1018–1026. https://doi.org/10.1109/58.655627, (1997).